Research Square

Preprints are preliminary reports that have not undergone peer review.
They should not be considered conclusive, used to inform clinical practice,
or referenced by the media as validated information.

Tailoring continuous dynamic recrystallization via initial microstructure regulation through Te addition in 6016 aluminum alloy

Yaoxin Li
Central South University
Yu Liu
csuliuyu@csu.edu.cn
Central South University
Wenqing Zhu
Central South University
Yuanchun Huang
Central South University
Changke Chen
Shihezi Zhonghe New Materials Co., Ltd
Xieyi Zhang
Collage of Shihezi University

Research Article

Keywords: 6016 aluminum alloy, microalloying, tellurium element, microstructure, hot deformation behavior

Posted Date: November 11th, 2026

DOI: https://doi.org/10.21203/rs.3.rs-11302148/v1

License: This work is licensed under a Creative Commons Attribution 4.0 International License.
Read Full License

Additional Declarations: No competing interests reported.

Tailoring continuous dynamic recrystallization via initial microstructure regulation through Te addition in 6016 aluminum alloy

Yaoxin Li[1]， Yu Liu[1*]， Wenqing Zhu[1]， Yuanchun Huang[1]， Changke Chen[2]， Xieyi Zhang[3]

1 Light Alloy Research Institute, Central South University, Changsha 410000, China

2 Shihezi Zhonghe New Materials Co., Ltd., Shihezi 832000,China

3 Chemistry and Chemical Engineering Collage of Shihezi University, Shihezi 832003, People's Republic of China

Corresponding author: LIU Yu E-mail: csuliuyu@csu.edu.cn

Abstract: This study investigates the effects of trace Te additions (0–0.6 wt.%) on the solidification, homogenization, and hot deformation behavior of 6016 aluminum alloys. In the as-cast state, Te disrupts the continuous interdendritic eutectic network and refines the dendrite structure, but the refinement saturates and slightly weakens above 0.4 wt.%. After homogenization, grain size first decreases and then marginally increases with Te content, with the 0.4 wt.% Te alloy exhibiting the finest and most uniform grain structure. Te is found to mainly exist in solid solution or as a highly dispersed state, indirectly optimizing the second-phase distribution. During hot compression at 450 °C, all alloys show clear strain-rate sensitivity. At 0.01 s^{-1}, the 0.4 wt.% Te alloy exhibits relatively lower flow stress, along with lower KAM values and a higher fraction of high-angle grain boundaries, indicating stronger dynamic softening and more pronounced continuous dynamic recrystallization. Overall, the 0.4 wt.% Te addition proves optimal, synergistically improving the microstructure and deformation behavior, which provides a valuable basis for the composition design of high-performance 6016 aluminum alloys.

Key words： 6016 aluminum alloy; microalloying; tellurium element; microstructure; hot deformation behavior

1. Introduction

Aluminum alloys have been widely used in automotive light-weighting owing to their low density, high specific strength, excellent corrosion resistance, and good formability[1,2,3]. Among them, Al-Mg-Si wrought aluminum alloys, such as 6016 alloy, are extensively employed for automotive body panels because of their favorable

combination of formability, bake-hardening response, and surface quality[4,5]. However, the final service performance of these alloys is governed not only by subsequent age-hardening precipitation behavior, but also by the characteristics of the as-cast microstructure, the homogenization process, and microstructural evolution during hot working[6,7]. Therefore, regulating the subsequent hot deformation behavior from the perspective of the initial microstructure is of great importance for optimizing the overall performance of the material[8,9].

In recent years, microalloying has been recognized as an effective strategy for tailoring the microstructure and properties of Al-Mg-Si aluminum alloys[10]. The introduction of minor alloying elements can markedly affect the solidification behavior of these alloys, including dendrite morphology evolution, eutectic microstructural characteristics, and the type and distribution of second phases. These changes further influence the dissolution, spheroidization, and coarsening of second phases during homogenization, thereby exerting a profound effect on the flow behavior and microstructural evolution during subsequent hot working[11,12] To date, extensive studies have been conducted on trace elements such as Sc, Zr, Er, Cr, and Sr, which have shown significant effects on grain refinement, precipitation strengthening, and microstructural stabilization[13[14,15]. It is well known that the addition of rare-earth Sc to Al-Mg-Si alloys can refine α-Al dendrites[16], improve the morphology of eutectic Si[17,18], affect precipitation behavior, and reduce Fe-containing phases[19], thereby effectively enhancing tensile strength and yield strength[20,21]. Zhao et al.[22] found that the addition of Zr and rare-earth Er to Al-Mg-Si aluminum alloys shortened the aging time and improved the age-hardening response. Tang et al.[23]reported that the addition of Cr and Sr significantly modified the morphology of Fe-rich phases: Cr promoted the transformation of β-AlFeSi into α-Al(FeCr)Si, whereas Sr reduced the phase size, leading to improved mechanical properties of high-Fe 6016 alloy. In contrast, studies on the role of Te in Al-Mg-Si alloys remain limited, and systematic investigations into its effects on the initial microstructure and hot deformation behavior are particularly lacking.

Tellurium is a trace element that has rarely been used in aluminum alloys, and its role during alloy solidification remains insufficiently reported. A limited number of studies

have suggested that Te may affect the evolution of the solidification microstructure and the formation and distribution of eutectic phases; however, direct evidence for its specific mechanism in aluminum alloys is still lacking. Accordingly, this study focuses on an Al-Mg-Si alloy and systematically investigates the effects of different Te contents on the as-cast microstructure and microstructural evolution during homogenization. Scanning electron microscopy and energy-dispersive spectroscopy were used to characterize the type, morphology, size, and distribution of second phases. High-temperature compression tests were further conducted to analyze differences in deformation behavior under different initial microstructural conditions. Based on these results, the relationship between Te-induced changes in the initial microstructure and the hot deformation behavior of the alloy was examined, with particular attention to the effects of second-phase distribution, kernel average misorientation (KAM), and grain-boundary misorientation on dynamic recovery and dynamic recrystallization. This study aims to clarify the microstructural regulation mechanism of Te microalloying in Al-Mg-Si alloys and its influence on hot-working behavior, thereby providing a theoretical basis for composition design and hot-processing optimization of this class of alloys.

2. Methodology

According to the designed compositions of the 6016 aluminum alloy samples, as-cast Al-Mg-Si-xTe alloys were prepared using an electric resistance furnace. The chemical compositions of the alloys were measured by optical emission spectroscopy (OES). The measured chemica of the alloys are listed in Table 1.

To eliminate compositional segregation in the as-cast microstructure and prevent local melting of low-melting-point eutectics, the as-cast alloy samples were homogenized at 550 °C for 10 h. This treatment largely promoted the homogenization and dispersed precipitation of second-phase particles, enhanced the microstructural stability of the matrix, and optimized the subsequent hot deformation response.

Table 1 Chemical compositions of experimental Al-Mg-Si-xTe alloys (wt.%)

Sample	Al/wt.%	Mg/wt.%	Si/wt.%	Te/wt.%
1#	Bal.	0.49	1.25	0
2#	Bal.	0.48	1.29	0.15

3#	Bal.	0.46	1.39	0.37
4#	Bal.	0.51	1.33	0.52

The homogenized samples were sectioned from the central region into 10 mm × 10 mm × 10 mm specimens by wire electrical discharge machining. The specimens were then ground and polished to a mirror finish, etched with Keller's reagent (95% H_2O + 2.5% HNO_3 + 1.5% HCl + 1% HF), and examined using an optical microscope (OLYMPUS). Backscattered electron (BSE) imaging was also performed using scanning electron microscopy (SEM) at 30 kV, combined with energy-dispersive X-ray spectroscopy (EDS) for compositional analysis, to characterize the morphology, size, and distribution of second-phase particles. To determine the existence form of Te in the alloy, the 0.6% Te alloy with the highest Te content was further analyzed by electron probe microanalysis (EPMA). EPMA was performed using a Shimadzu EPMA-1720T electron probe microanalyzer at an accelerating voltage of 15 kV and a beam current of 100 nA, with an electron beam spot diameter of approximately 1 μm.

Cylindrical specimens with a diameter of 10 mm and a height of 15 mm were prepared from the 0.5R position of the homogenized ingots. Hot compression tests were conducted using a Gleeble-3800 thermomechanical simulator, as shown in Fig. 1a,b. Because hot working of 6xxx-series aluminum alloys is commonly performed at approximately 400-500 °C, 450 °C lies within the typical hot deformation temperature range and is suitable for observing microstructural evolution associated with dynamic recovery and dynamic recrystallization[24]. This temperature is also below the range in which local melting may occur, thereby ensuring stable compression deformation. Therefore, the deformation temperature was set to 450 °C, and strain rates of 0.001, 0.01, 0.1, 1, and 10 s^{-1} were applied. Each specimen was heated to the deformation temperature at a rate of 10 °C/s, held for 180 s to ensure thermal homogenization, and then axially compressed to a 60% reduction in height. Immediately after deformation, the specimens were quenched to room temperature to preserve the high-temperature microstructure. The deformed specimens were then sectioned longitudinally along the compression axis, and the central plane (Fig. 1c) was prepared for electron backscatter diffraction (EBSD) analysis. The specimens were mechanically polished and subsequently electropolished in a solution of 10% $HClO_4$ + 90% C_2H_5OH at 20 V and

-15 °C. EBSD data were collected using a Nordlys Max2 detector attached to a field-emission SEM, with a step size of 2.5 μm, and were processed using Channel 5 software.

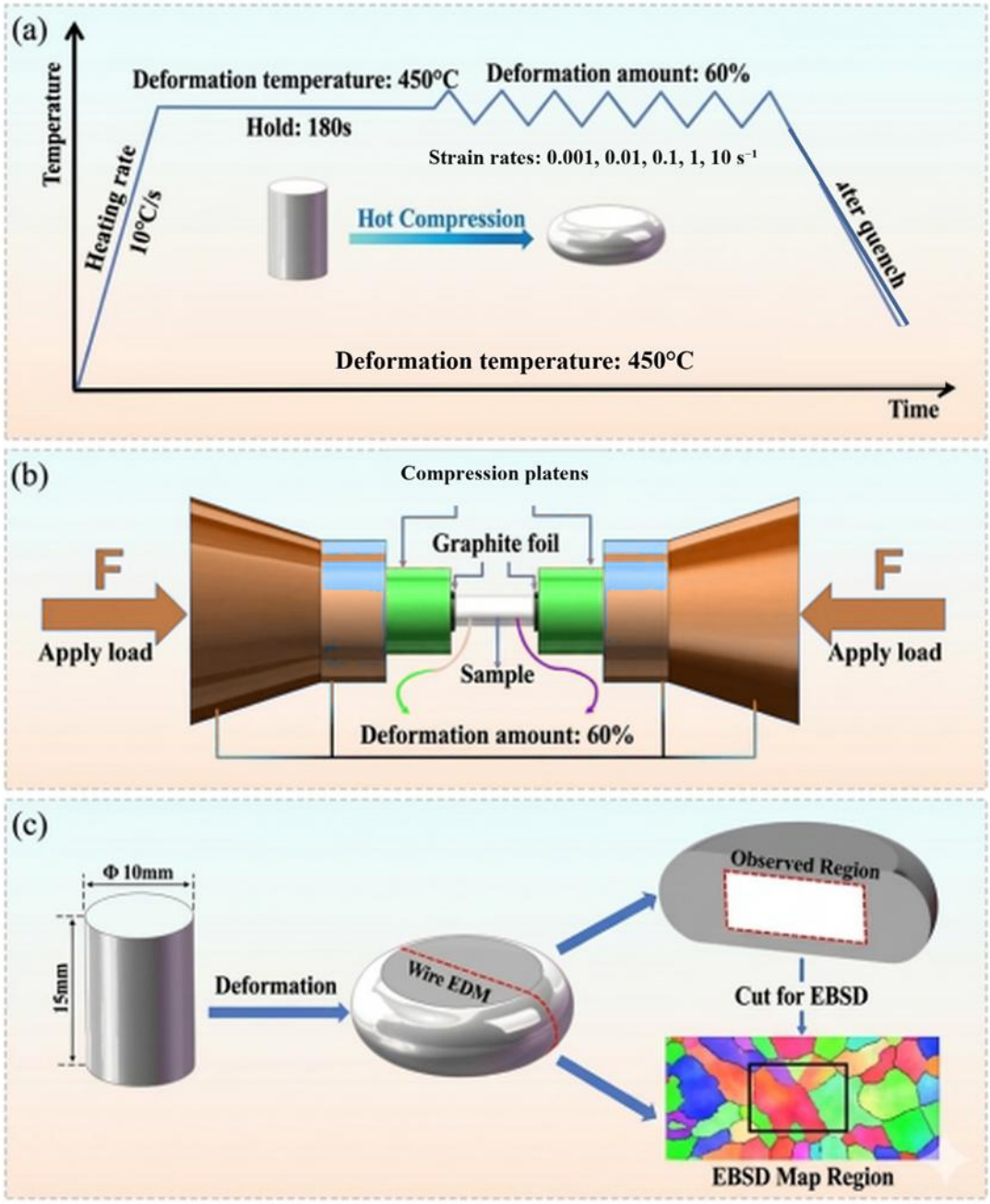


Fig.1 Schematic diagram of the hot compression process, (a) hot compression process;(b) schematic illustration of hot compression;(c) microstructural observation plane of the sample

3. Results and Discussion

3.1 As-cast microstructure

Fig. 2 shows the as-cast metallographic microstructures of 6016 aluminum alloys with different Te contents. Overall, all samples consist of an α-Al matrix and eutectic

structures distributed along the interdendritic regions, exhibiting typical dendritic solidification characteristics. With increasing Te content, pronounced changes occur in both dendrite morphology and eutectic distribution. In the alloy without Te addition, the microstructure shows a coarse dendritic structure with clear dendrite outlines and well-developed secondary dendrite arms. A large amount of continuously distributed eutectic structure is present in the interdendritic regions, appearing as a network-like or skeleton-like morphology. This eutectic structure is mainly dominated by the Si phase and forms continuous paths along grain boundaries, indicating significant segregation of solute elements, especially Si, into the interdendritic regions during solidification. The presence of a continuous eutectic network may act as a stress concentration site during subsequent deformation, which is detrimental to ductility.

After the addition of a small amount of Te, the dendritic structure becomes refined, and the dendrite outlines become less distinct. Meanwhile, the originally continuous eutectic network is clearly fragmented and becomes more discrete. Some eutectic regions change from elongated strips to shorter lamellar or discontinuous distributions. This indicates that Te addition suppresses, to some extent, the continuous growth of the eutectic structure and reduces elemental segregation. As the Te content further increases, the dendritic structure is further refined and locally shows a tendency toward equiaxed morphology, while the original dendritic skeleton is weakened and the microstructure becomes more uniform. These results suggest that Te has a refining effect on the solidification microstructure. At this stage, the connectivity of the eutectic structure is disrupted, leading to a relatively isolated particle-like distribution. With further addition of 0.6% Te, the eutectic structure becomes more evidently discrete; however, the dendrites are slightly coarser than those in the 0.4% Te alloy, and the boundaries become slightly blurred.

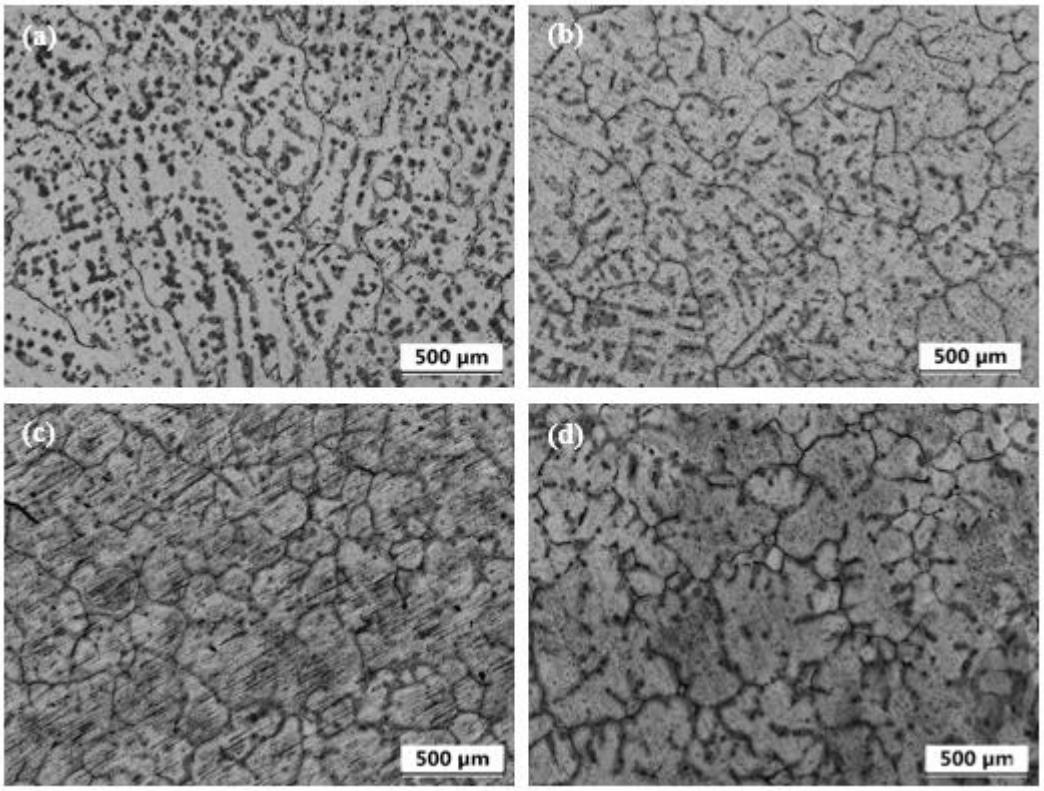


Fig.2 Metallographic microstructures of as-cast 6016 aluminum alloys with different Te contents

（a）0%Te；（b）0.2%Te;（c）0.4%Te；（d）0.6%Te

Fig. 3 shows SEM images and corresponding EDS mapping results of the as-cast samples with different Te contents, where Fig. 3a-d correspond to Te contents of 0%, 0.2%, 0.4%, and 0.6%, respectively. Overall, the second phases in the as-cast 6016 alloy are mainly Si-rich phases and are preferentially distributed in the interdendritic regions. The addition of Te markedly changes the distribution of these Si-rich phases. In the alloy without Te addition, the Si phase exhibits a continuous network-like distribution, showing a typical eutectic morphology. With increasing Te content, this network structure is gradually fragmented and transformed into short-chain and discrete particle-like distributions, indicating that Te can effectively suppress the continuous growth of eutectic Si. Meanwhile, Mg does not show obvious enrichment regions. In addition, no distinct Te-enriched regions are observed at the SEM-EDS characterization scale, suggesting that Te does not form enrichment phases resolvable by SEM-EDS. Considering the low Te addition and the limited capability of SEM-EDS for detecting trace, dispersed, or solid-solution elements, together with the systematic changes in

dendrite morphology, eutectic continuity, and second-phase distribution with Te content, Te may modify solute redistribution and eutectic microstructural evolution during solidification. Its specific existence form still requires further confirmation by higher-resolution characterization.

Point EDS analysis of selected regions was further performed, and the results are listed in Table 2. The Si content is generally higher than the Mg content at the analyzed points, and the Mg/Si ratio does not correspond to the stoichiometry of Mg_2Si. Based on the compositional characteristics, the second phases can be classified into three types. The first type is Si-rich regions, with Si contents above 30 at.%, indicating that eutectic Si is the dominant phase. The second type is Mg-Si co-enriched regions, in which both Mg and Si contents increase but do not satisfy the stoichiometric ratio. The third type consists of complex Al-dominated second phases containing Fe.

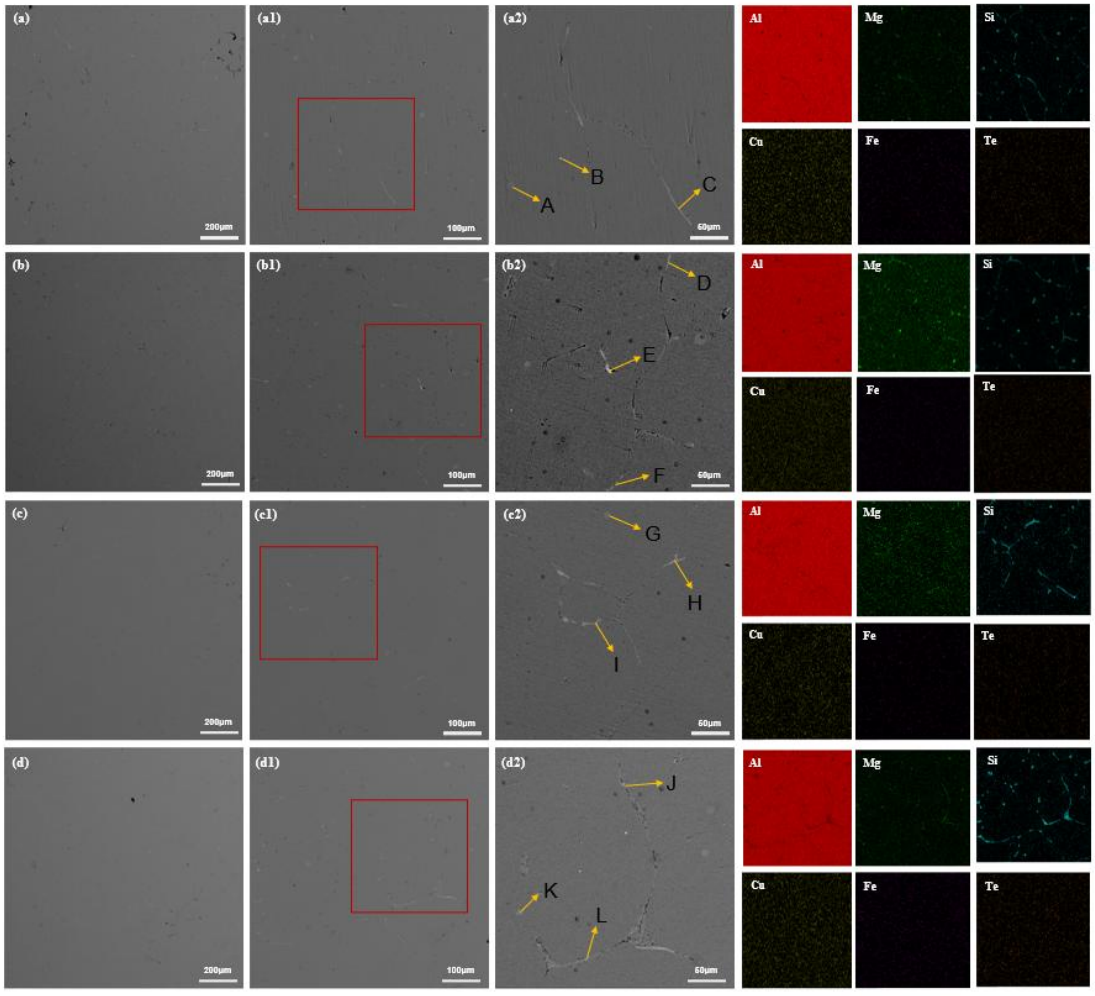


Fig.3 SEM images and EDS mapping analysis of as-cast 6016 aluminum alloys with different Te contents

（a,a1,a2）0%Te；（b,b1,b2）0.2%Te;（c,c1,c2）0.4%Te；（d,d1,d2）0.6%Te

Table 2 Chemical investigations of intermetallic particles,as shown in Figure 3

		Atomic%					
		Al	Si	Mg	Fe	Cu	Te
Te-free	A	50.8	34.1	14.0	1.1	0.1	0
	B	64.0	21.0	8.3	6.5	0.2	0
	C	56.0	35.0	7.1	1.7	0.1	0
0.2%Te	D	66.5	18.5	11.2	3.5	0.1	0
	E	67.2	26.5	5.2	1.0	0	0
	F	61.4	27.6	4.3	6.7	0	0
0.4%Te	G	55.3	30.0	13.4	1.1	0.1	0.1
	H	58.4	23.6	13.7	4.2	0.1	0
	I	74.6	15.8	7.4	2.1	0	0
0.6%Te	J	66.2	29.3	3.4	1.0	0	0.1
	K	71.4	19.3	6.8	2.6	0	0
	L	51.1	46.4	2.5	0	0	0

3.2 Homogenized microstructure

Four groups of as-cast 6016 aluminum alloy samples with different Te contents were selected and subjected to homogenization treatment to investigate the effect of Te content on the homogenized microstructure of 6016 alloy and to compare the microstructural differences between the as-cast and homogenized states. As shown in Fig. 4, the grain size and distribution of the homogenized 6016 aluminum alloys exhibit a clear dependence on Te content. The alloy without Te addition shows relatively coarse grains. When the Te content is increased to 0.2%, the grain size decreases. At a Te content of 0.4%, the alloy exhibits a relatively finer and more uniform grain structure. However, when the Te content is further increased to 0.6%, the grain size increases to some extent, and the local microstructural uniformity slightly decreases.

The grain size of the alloys with different Te contents was statistically analyzed based on the metallographic microstructures. As shown in Fig. 5, the average grain size first decreases and then increases with increasing Te content. The 0.4% Te alloy exhibits the

smallest average grain size, indicating that an appropriate Te addition is beneficial for refining the homogenized microstructure.

In terms of grain size distribution, the 0.4% Te alloy shows better microstructural uniformity, with a concentrated grain size distribution and no obvious coarse grains or abnormal grain growth. In contrast, the alloys with other compositions exhibit grain size inhomogeneity or local coarsening to varying degrees. In addition, a small amount of second phases can be observed at the optical microscopy scale, mainly distributed within grains, without obvious continuous distribution along grain boundaries.

Overall, with increasing Te content, the grain size of the alloy follows a trend of initial refinement, optimum refinement, and subsequent coarsening, with the 0.4% Te alloy showing the most pronounced grain-refining effect. This fine and uniform initial microstructure implies a higher grain boundary density, which can provide more nucleation sites during subsequent hot deformation and thereby promote dynamic recrystallization. These features establish a microstructural basis for the subsequent evolution of the alloy and the associated changes in mechanical behavior.

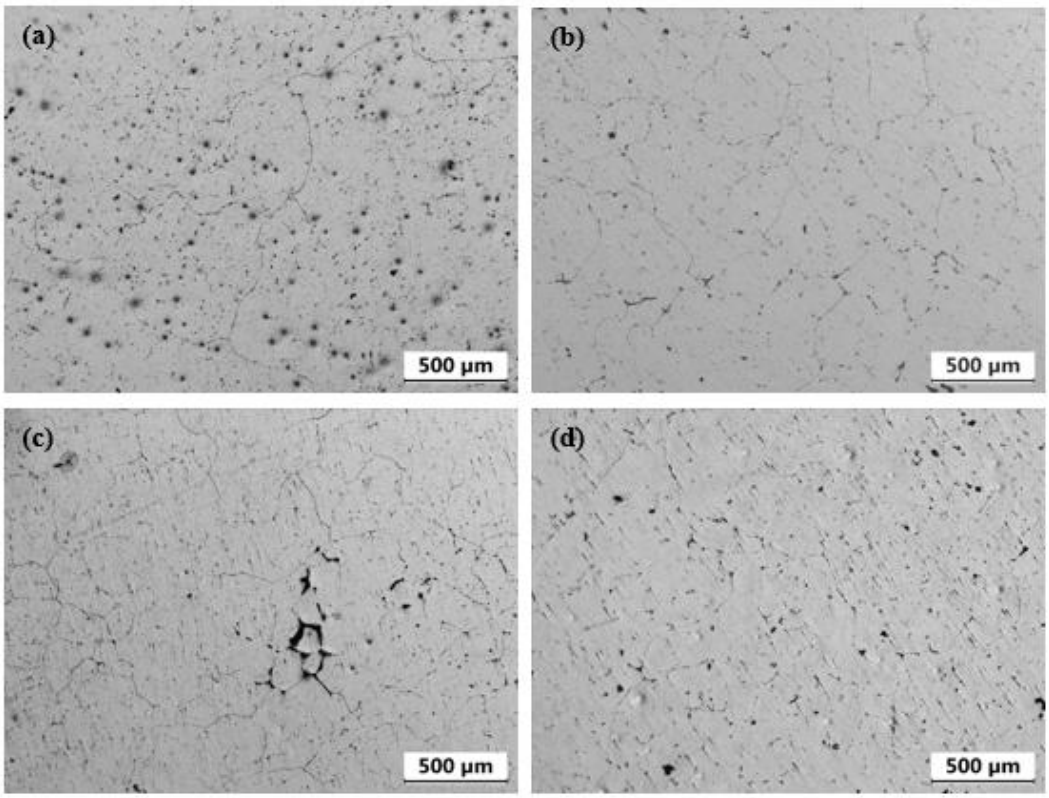


Fig.4 Metallographic images of homogenized 6016 aluminum alloys with different Te contents

（a）0%Te;（b）0.2%Te;（c）0.4%Te;（d）0.6%Te

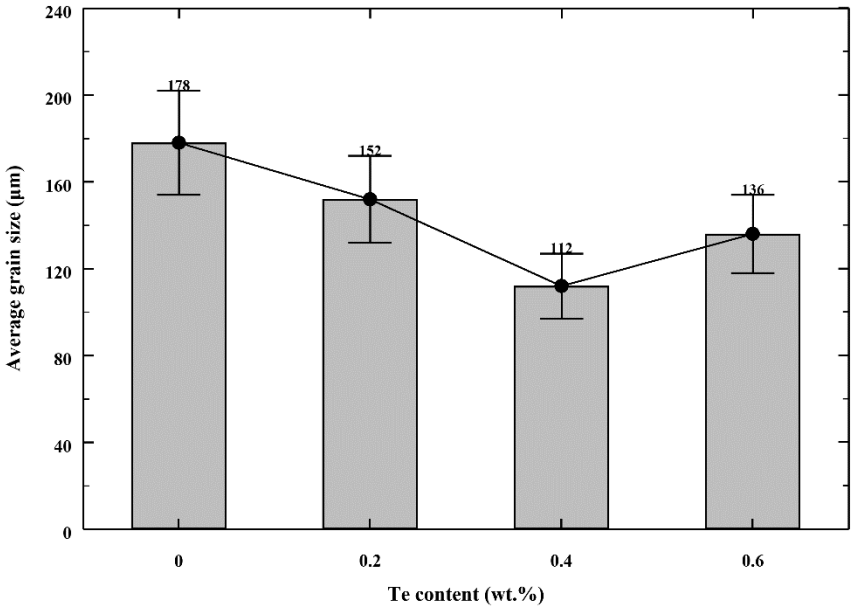


Fig.5 Grain size from metallographic images of homogenized 6016 aluminum alloys with different Te contents

Fig. 6 shows the SEM microstructures of the alloys with different Te contents after homogenization, where Fig. 6a-d correspond to Te contents of 0%, 0.2%, 0.4%, and 0.6%, respectively. All samples are mainly composed of an α-Al matrix, with a small number of bright white second-phase particles distributed within the matrix. These particles mainly exhibit short rod-like, needle-like, and particle-like morphologies and are mostly dispersed throughout the matrix. Based on the compositional characteristics of the analyzed points listed in Table 3, the second phases in the homogenized state can be classified into three types: Si-rich phases, Mg-Si co-enriched phases, and a small number of Fe-containing complex second phases.

A comparison of the microstructures of alloys with different Te contents reveals clear differences in the amount and distribution of second phases. As shown in Fig. 7, statistical analysis was performed based on Fig. 6a1-d1, only a small number of second-phase particles can be observed in the alloy without Te addition. After the addition of 0.2% Te, the number of second phases increases markedly. As the Te content further increases to 0.4%, the number of second phases increases again, and the particles exhibit a more dispersed distribution. However, when the Te content is increased to 0.6%, the number of second phases decreases compared with the previous condition,

accompanied by second-phase agglomeration and local clustering.

Therefore, according to the statistical results of the average equivalent diameter, number density, and area fraction of second phases in Fig. 7, the second-phase particles in the 0.4% Te alloy generally exhibit relatively small sizes and a more uniform distribution. In contrast, the 0.2% Te and 0.6% Te alloys show inhomogeneous distribution and local clustering, respectively. The dispersed second-phase particles can effectively pin grain boundaries and thus inhibit grain growth, which is consistent with the OM observation that the 0.4% Te alloy has the finest and most uniformly distributed grains. In addition, fine and dispersed second phases may influence the dislocation distribution during hot deformation and provide favorable conditions for subgrain formation and continuous dynamic recrystallization.

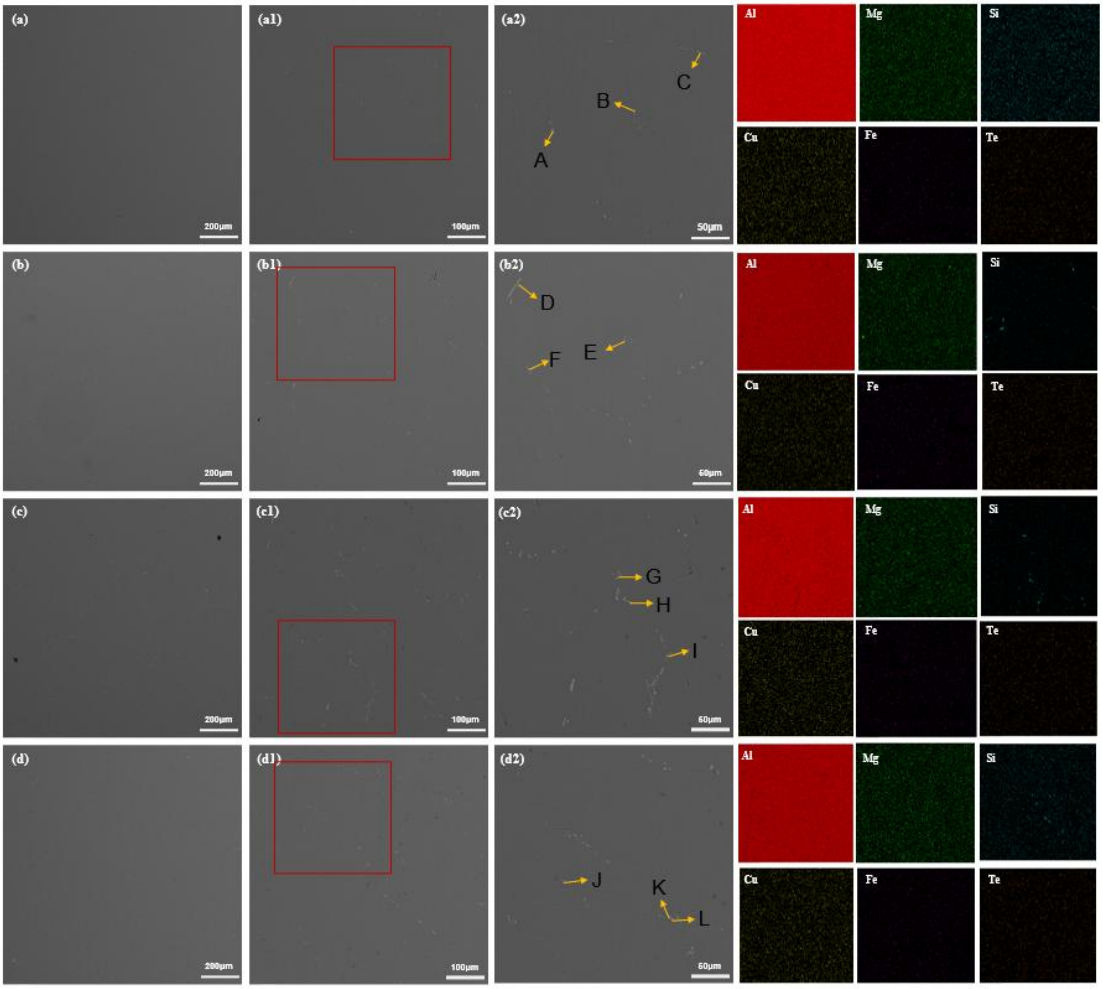


Fig.6 SEM images and EDS mapping analysis of homogenized 6016 aluminum alloys with different Te contents

（a,a1,a2）0%Te;（b,b1,b2）0.2%Te;（c,c1,c2）0.4%Te;（d,d1,d2）0.6%Te

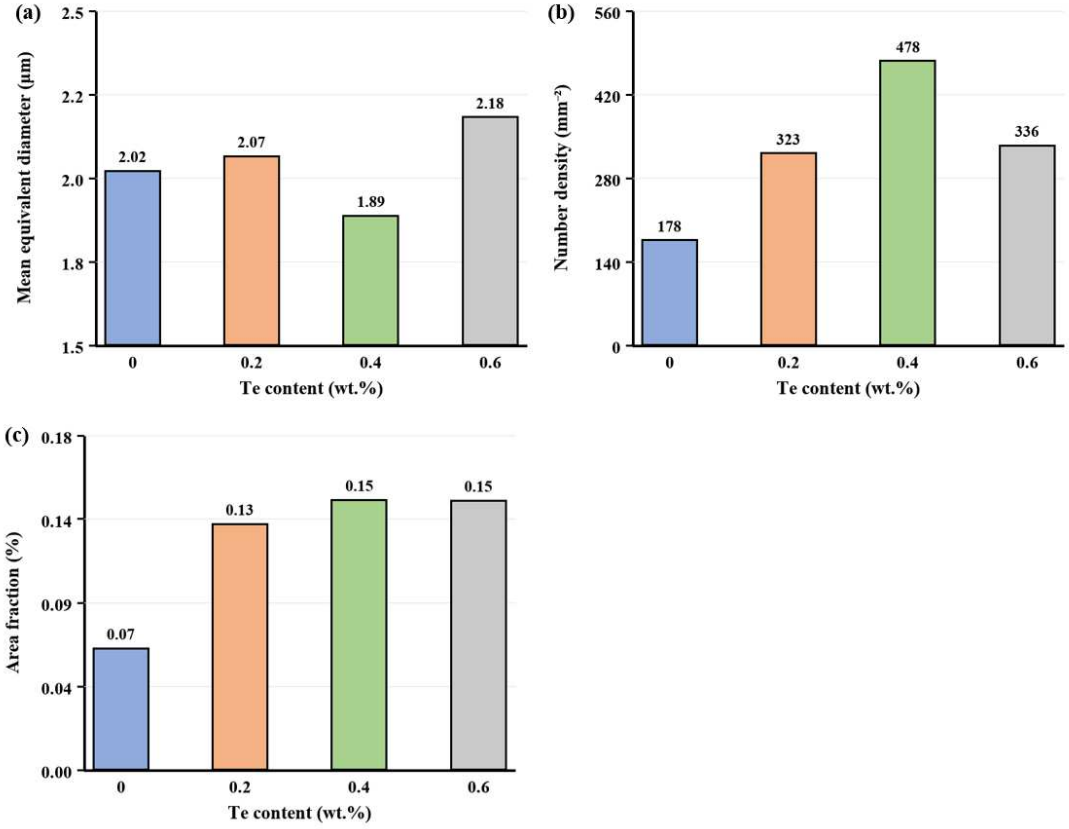


Fig.7 Mean equivalent diameter (a) ,number density (b) ,and area fraction of second-phase particles (c) in SEM images of homogenized 6016 aluminum alloys with different Te contents

Table 3 Chemical investigations of intermetallic particles,as shown in Figure 6

		Atomic%					
		Al	Si	Mg	Fe	Cu	Te
Te-free	A	66.9	19.7	9.8	3.6	0	0
	B	76.9	14.9	5.9	2.2	0	0
	C	95.1	2.7	0.8	1.3	0	0
0.2%Te	D	75.4	15.6	6.8	2.1	0.1	0
	E	66.6	16.7	9.4	2.4	4.9	0
	F	49.1	49.7	0.3	0	0.9	0
0.4%Te	G	78.8	13.4	5.9	1.9	0	0
	H	54.1	44.4	0.3	0	1.1	0
	I	63.1	22.4	10.7	3.6	0.2	0
0.6%Te	J	91.4	4.5	0.7	3.2	0.3	0
	K	90.0	5.4	0.6	0	4.0	0

L	39.5	57.6	0.3	0	2.5	0

Because no obvious Te-enriched phase was observed at the SEM-EDS characterization scale, it is difficult to directly determine the existence form of Te in the alloy. Therefore, the 0.6% Te alloy with the highest Te content was further selected for EPMA analysis to improve the identification of the Te distribution state. As shown in Fig. 8, the Te Lα signal is generally weak but is approximately uniformly distributed within the observed region, without obvious Te-enriched regions or continuous segregation bands. Combined with the SEM-EDS results, this indicates that, at the characterization scale used in this study, Te does not form micrometer-scale resolvable enriched phases but exists in the α-Al matrix in a relatively uniform solid-solution state.

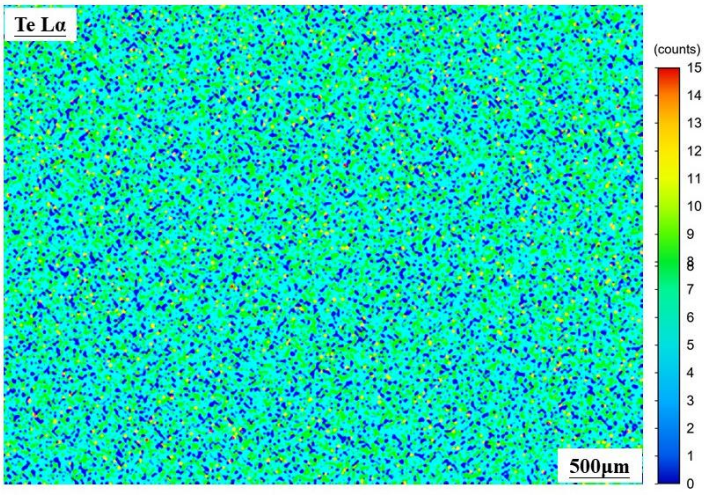


Fig.8 EPMA of Te distribution in the homogenized 0.6 wt.% Te alloy

3.3 Hot compression flow behavior

Fig. 9 shows the true stress-true strain curves of 6016 aluminum alloys with different Te contents deformed at 450 °C under different strain rates (0.001-10 s^{-1})[24]. Overall, all alloys exhibit typical flow behavior during hot deformation. At the initial stage of deformation, the stress increases rapidly with increasing strain, indicating that work hardening is dominant. According to the general hot deformation behavior of aluminum alloys, this stage is usually associated with rapid dislocation multiplication and enhanced dislocation interactions[25]. With further increasing strain, the rate of stress increase gradually decreases, as the dislocation multiplication rate progressively

approaches a balance with the dynamic recovery rate, causing the stress-strain curves to enter a relatively steady stage. When the strain continues to increase, the stress becomes nearly stable or even decreases slightly, suggesting that dynamic softening gradually becomes dominant. Because aluminum alloys have high stacking fault energy, dynamic recovery is usually the main softening mechanism during hot deformation, which is also an important reason why no obvious peak softening feature appears in the curves[26].

The strain rate has a pronounced effect on the flow behavior of the alloys. With increasing strain rate, the flow stress generally increases[27,28]. This is mainly because, under higher strain-rate conditions, dislocations have insufficient time to be annihilated through climb and cross-slip, leading to rapid dislocation accumulation and enhanced work hardening. In addition, a higher strain rate shortens the time available for dynamic recovery and dynamic recrystallization, thereby further increasing the deformation resistance of the material.

At a strain rate of 0.01 s^{-1}, the alloys with different Te contents exhibit pronounced differences in flow stress. Among the different compositions, the 0.2% Te alloy shows the highest flow stress, whereas the 0.4% Te alloy exhibits the lowest flow stress. This result indicates that, at 0.01 s^{-1}, the 0.4% Te alloy has the lowest deformation resistance and undergoes the most sufficient dynamic softening. Combined with the SEM and EBSD results, this behavior is closely related to second-phase distribution and recrystallization behavior. In the 0.4% Te alloy, the second-phase particles are relatively fine and more dispersively distributed, which may facilitate a more uniform dislocation distribution and subgrain evolution during deformation, thereby promoting continuous dynamic recrystallization. This inference is consistent with the subsequent EBSD results, in which the 0.4% Te alloy exhibits a lower kernel average misorientation (KAM) value and a higher fraction of high-angle grain boundaries. In contrast, the inhomogeneous distribution of second phases in the 0.2% Te alloy makes it difficult to effectively promote recrystallization and locally impedes dislocation motion, resulting in increased dislocation accumulation and higher flow stress. Therefore, at this strain rate, dynamic recovery and continuous dynamic recrystallization are the dominant softening mechanisms, and the 0.4% Te alloy exhibits the most favorable deformation

softening behavior owing to its optimized second-phase regulation.

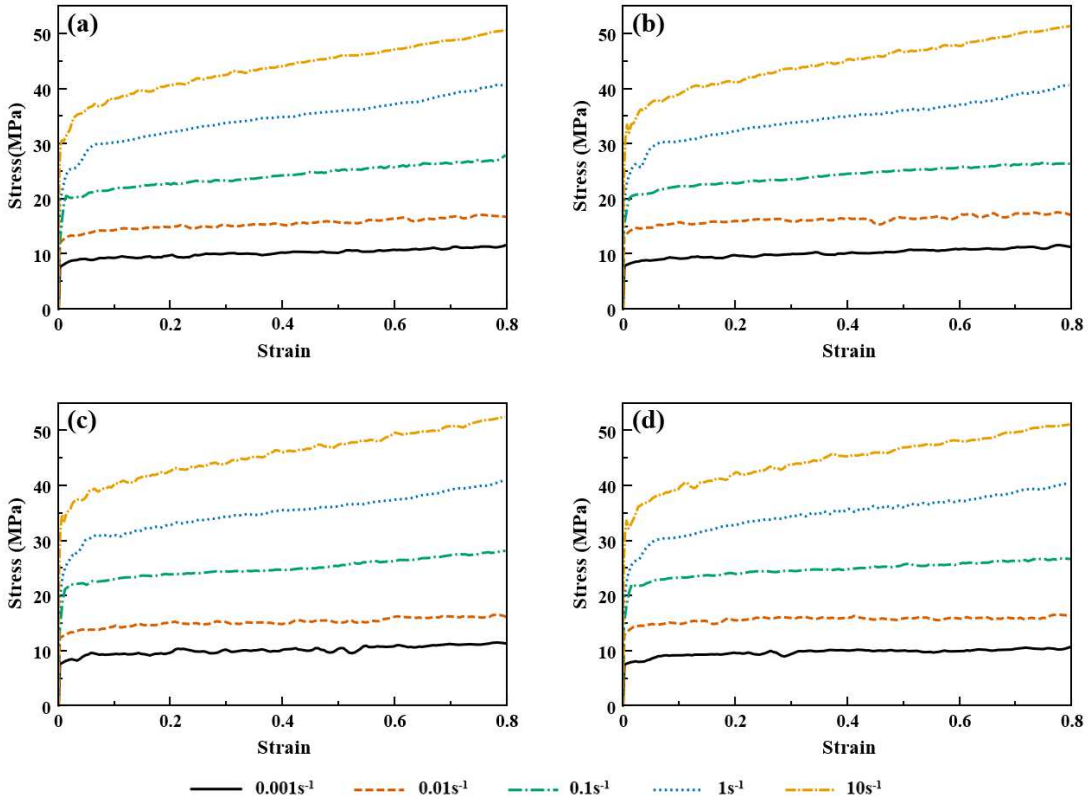


Fig.9 Stress-strain curves at different strain rates for various Te contents

（a）0%Te;（b）0.2%Te;（c）0.4%Te;（d）0.6%Te

3.4 Deformed microstructure and dynamic recrystallization

To further compare the effect of Te content on the flow behavior of the alloy, a representative strain rate of 0.01 s^{-1} was selected for detailed analysis. At this strain rate, the stress-strain curves show clear work-hardening behavior while also exhibiting a certain degree of dynamic softening, making them more suitable for analyzing the hot deformation mechanism of the material. In addition, this strain-rate range is relatively close to the deformation conditions used in practical hot working, and therefore has certain engineering relevance. Fig. 10 shows the EBSD orientation maps and corresponding grain-boundary misorientation distributions of the alloys with different Te contents after hot compression at a strain rate of 0.01 s^{-1}. The orientation maps show that all alloys exhibit typical hot-deformed microstructures, with grains elongated along the deformation direction and accompanied by varying degrees of intragranular orientation gradients, indicating significant dislocation accumulation and substructure evolution during deformation.

This result indicates that the 0.4% Te alloy undergoes more sufficient dynamic recrystallization under this deformation condition. During hot deformation, low-angle grain boundaries mainly originate from dislocation accumulation and rearrangement, reflecting the deformation stored energy within the material, whereas high-angle grain boundaries are generally formed through subgrain rotation and are an important feature of continuous dynamic recrystallization. Therefore, a lower fraction of low-angle grain boundaries and a higher fraction of high-angle grain boundaries indicate a higher degree of recrystallization and more sufficient dislocation annihilation. Combined with the SEM results, the second-phase particles in the 0.4% Te alloy are relatively fine and dispersively distributed, which may facilitate a more uniform dislocation distribution and the formation and evolution of subgrain structures. As subgrains gradually rotate and transform into high-angle grain boundaries, continuous dynamic recrystallization is promoted. In contrast, the 0.2% Te and 0.6% Te alloys exhibit higher fractions of low-angle grain boundaries, indicating more pronounced dislocation accumulation and a relatively lower degree of recrystallization. This may be related to the inhomogeneous distribution or agglomeration of second phases, which restricts subgrain evolution and thereby inhibits the formation of high-angle grain boundaries.

This result is consistent with the flow-curve analysis, in which the 0.4% Te alloy exhibits the lowest flow stress at 0.01 s^{-1}. This behavior is attributed to its higher fraction of high-angle grain boundaries and lower dislocation density, which enable more sufficient dynamic softening and thus reduce the deformation resistance. Therefore, at a Te content of 0.4%, the distribution state of second phases is effectively regulated, promoting continuous dynamic recrystallization, increasing the fraction of high-angle grain boundaries, and reducing the dislocation density, thereby markedly improving the hot deformation performance of the alloy.

It should be noted that the low-angle grain boundary (LAGB) fraction of the 0.2% Te alloy is 89.10%, higher than that of the alloy without Te addition (83.90%), indicating that a small amount of Te does not monotonically promote dynamic recrystallization. Instead, the higher LAGB fraction in the 0.2% Te alloy indicates that more subgrain boundaries and local misorientations remain after deformation, suggesting that continuous dynamic recrystallization is incomplete. This result

demonstrates that the effect of Te on the deformed microstructure is strongly content-dependent rather than a simple positive promotion effect. Only at a Te content of 0.4% does the LAGB fraction decrease to 78.22%, accompanied by a corresponding increase in the HAGB fraction, indicating a more complete transformation from subgrain boundaries to high-angle grain boundaries.

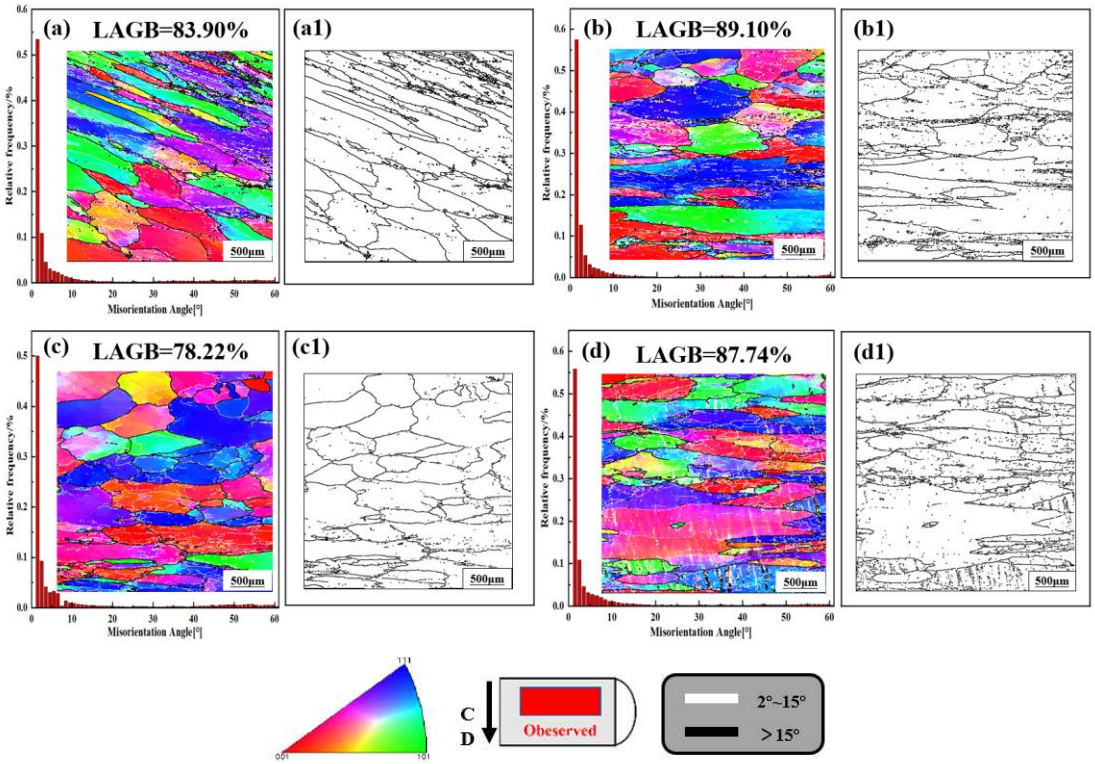


Fig.10 IPF maps and corresponding grain boundary misorientation angle distributions of 6016 aluminum alloys with different Te contents

（a,a1）0%Te;（b,b1）0.2%Te;（c,c1）0.4%Te;（d,d1）0.6%Te

To further characterize the dislocation distribution characteristics of 6016 aluminum alloys with different Te contents during hot deformation, kernel average misorientation (KAM) analysis was performed, as shown in Fig. 11. The KAM value is commonly used to reflect local intragranular orientation differences and is closely related to the density of geometrically necessary dislocations. A higher KAM value indicates more severe dislocation accumulation and greater deformation inhomogeneity.

The KAM distribution maps and statistical results show clear differences in KAM values among the alloys with different Te contents. The average KAM values of the 0%, 0.2%, 0.4%, and 0.6% Te alloys are approximately 0.71, 0.81, 0.65, and 0.78, respectively. Among them, the 0.4% Te alloy exhibits the lowest KAM value, whereas

the 0.2% Te alloy shows the highest value. This result indicates that the 0.4% Te alloy has the lowest dislocation density during deformation and undergoes the most sufficient dynamic softening.

Combined with the grain-boundary analysis above, the 0.4% Te alloy exhibits the lowest fraction of low-angle grain boundaries and the highest fraction of high-angle grain boundaries, indicating that continuous dynamic recrystallization is more sufficient in this alloy. During this process, dislocations are continuously eliminated through slip, climb, and annihilation, reducing intragranular orientation gradients and resulting in a lower KAM value. In addition, SEM analysis shows that the second-phase particles in the 0.4% Te alloy are fine and dispersively distributed. This microstructural feature is favorable for promoting a uniform dislocation distribution and stable subgrain evolution. During hot deformation, subgrains gradually rotate and transform into high-angle grain boundaries, thereby accelerating recrystallization and reducing dislocation density.

In contrast, the 0.2% Te and 0.6% Te alloys show higher KAM values, indicating that higher local misorientation and geometrically necessary dislocation density are retained after deformation. Combined with the SEM observations, this may be related to the inhomogeneous distribution or local clustering of second phases, which reduces local deformation compatibility and suppresses dynamic recovery and continuous dynamic recrystallization. This result is highly consistent with the flow-curve analysis, in which the 0.4% Te alloy exhibits the lowest flow stress at a strain rate of 0.01 s^{-1}. This is because its lower dislocation density and more sufficient dynamic softening significantly reduce deformation resistance, whereas the severe dislocation accumulation in the 0.2% Te alloy leads to the highest deformation resistance. Therefore, the KAM analysis further demonstrates that an appropriate Te content (0.4%) promotes continuous dynamic recrystallization and effectively reduces dislocation density by regulating the second-phase distribution, thereby markedly improving the hot deformation behavior of the alloy.

In addition, the KAM value reflects local intragranular misorientation and the density of geometrically necessary dislocations, whereas the LAGB fraction represents the proportion of low-angle subgrain boundaries. These two parameters are usually

correlated, but they do not have a strict one-to-one correspondence. The 0% Te alloy shows higher LAGB fraction and KAM value than the 0.4% Te alloy, indicating that more low-angle substructures and higher local misorientation are retained after deformation. In contrast, the 0.4% Te alloy simultaneously exhibits a lower LAGB fraction, a higher HAGB fraction, and a lower KAM value, suggesting that the transformation of some low-angle subgrain boundaries into high-angle grain boundaries is more complete and that the local dislocation density is relatively lower. Therefore, the combined changes in LAGB fraction and KAM value support the conclusion that the 0.4% Te alloy undergoes more sufficient dynamic recovery and continuous dynamic recrystallization at 0.01 s^{-1}.

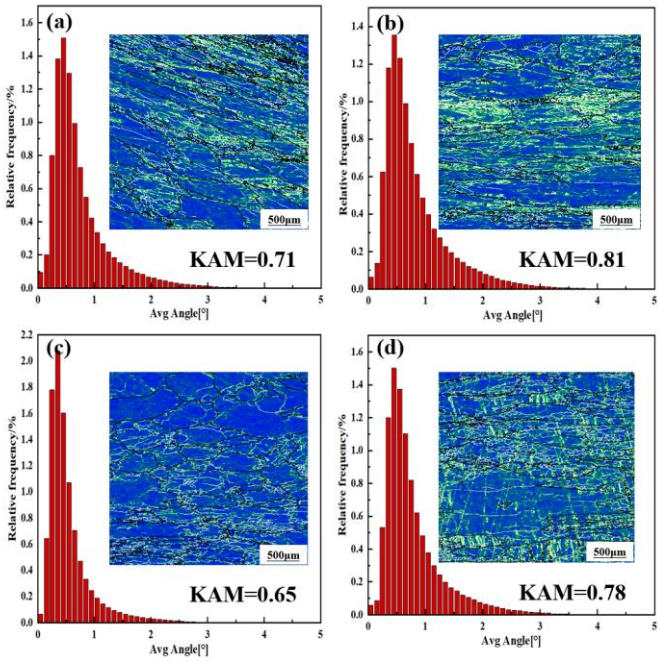


Fig.11 KAM maps, corresponding KAM distributions, and average KAM values of 6016 aluminum alloys with different Te contents

（a）0%Te;（b）0.2%Te;（c）0.4%Te;（d）0.6%Te

4. Conclusions

This study investigated the effects of Te additions (0–0.6 wt.%) on the solidification microstructure, homogenized microstructure, and high-temperature deformation behavior of 6016 aluminum alloy. The main conclusions are as follows:

(1) Te addition disrupts the continuous interdendritic eutectic network, promotes a more discrete distribution of second-phase particles, and refines the dendritic structure. These effects intensify with increasing Te content up to 0.4 wt.%, beyond which saturation and slight weakening occur. The 0.4 wt.% Te alloy exhibits the best as-cast microstructural uniformity.

(2) With increasing Te content, the grain size first decreases and then increases, exhibiting a non-monotonic trend. The 0.4 wt.% Te alloy shows the finest and most uniform grain structure. The second phases can be classified into three types, while no independent Te-rich phase is detected by SEM-EDS. EPMA analysis reveals that Te is uniformly distributed in the α-Al matrix in a solid-solution state, suggesting that Te exerts its microstructural regulation indirectly by influencing solute redistribution and second-phase evolution.

(3) During hot compression at 450 °C, all alloys exhibit significant strain-rate sensitivity, with flow stress increasing with strain rate. At the same strain rate, the flow stress varies among alloys with different Te contents. The 0.4 wt.% Te alloy shows relatively lower flow stress at the low strain rate of 0.01 s^{-1}.

(4) EBSD analysis at 0.01 s^{-1} reveals that the 0.4 wt.% Te alloy possesses the lowest KAM value and the highest fraction of high-angle grain boundaries, indicating more sufficient dynamic softening and more pronounced continuous dynamic recrystallization (CDRX) characteristics. Combined with the as-cast and homogenized results, the mechanism by which Te promotes CDRX can be attributed to the stepwise optimization of the initial microstructure—including dendrite refinement, eutectic network disruption, grain refinement, and second-phase dispersion—which provides more uniform microstructural conditions for subsequent hot deformation.

Acknowledgments

The authors acknowledge the financial support from Bintuan Science and Techn ology Program(2023AA003), Shanxi Provincial Major Science and Technology Special Project (202401050201003), and CZ003146 Tianchi Talent Young Doct or RCZK202524 Shihezi University High-Level Talent Project. Also, this work was and was supported in part by the High-Performance Computing Center of

Central South University.

Conflicts of Interest

The authors declare no conflict of interest.

Data availability

The datasets generated during and/or analysed during the current study are avai lable from the corresponding author on reasonable request.

Author contributions

Yu Liu: Conceptualization, Investigation, Software, Validation, Review. Yaoxin LI: Investigation, Software, Validation, Writing – original draft. Yuanchun Huan g: Conceptualization, review& editing. Wenqing ZHU: Validation, Software. Cha ngke Chen: Validation, Software. Xieyi Zhang: Validation, Software.

Ethics approval

Not applicable for the submitted paper.

Consent to Participate, and Consent to Publish

All authors have approved this manuscript and agree to journal´s submission policies.

References

[1] Wei Z L. Brief discussion on the influence of aluminum alloy component s on automotive lightweighting [J]. China Plant Engineering, 2022(6): 139 -141. (in Chinese)

[2] Sun H Y. Application of aluminum alloys in modern automotive lightweig ht production [J]. Modern Industrial Economy and Informationization, 202 2, 12(2): 135-138. (in Chinese)

[3] Busarac N, Adamovic D, Grujovic N, et al. Lightweight materials for aut omobiles[C]//IOP Conference Series: Materials Science and Engineering. I OP Publishing, 2022, 1271(1): 012010.

[4] Ghosh M , Miroux A , Werkhoven R J ,et al.Warm deep-drawing and po st drawing analysis of two Al-Mg-Si alloys[J].Journal of Materials Process ing Technology, 2014, 214(4):756-766.DOI:10.1016/j.jmatprotec.2013.10.020.

[5] Bhat K U, Panemangalore D B, Kuruveri S B, et al. Surface modificatio n of 6xxx Series aluminum alloys[J]. Coatings, 2022, 12(2): 180.

[6] Guo F J, Ma F, Chi R, et al. Microstructural evolution during the prepar ation of Al-Mg-Si alloy sheets [J]. Hot Working Technology, 2023, 52(15): 26-30. (in Chinese)

[7] Li Y X, Wang C Y. Research status of production technology for 6016 a luminum alloy automotive sheets [J]. Automobile Technology & Material, 2025(1): 46-55. (in Chinese)

[8] Li J , Wu X , Cao L ,et al.Hot deformation and dynamic recrystallization in Al-Mg-Si alloy[J].Materials Characterization, 2021, 173(1):110976.DOI: 10.1016/j.matchar.2021.110976.
[9] P. Snopiński,M. Król,T. Tański,et al.Effect of initial microstructure on hot deformation behavior of AlMg5Si2Mn alloy[J].Materials Characterization, 2021, 177:111167-.
[10] Callegari B , Lima T N , Coelho R S .The Influence of Alloying Elements on the Microstructure and Properties of Al-Si-Based Casting Alloys: A Review[J].Metals (2075-4701), 2023, 13(7).DOI:10.3390/met13071174.
[11] Cui S , Mishra R , Jung I H .Thermodynamic analysis of 6xxx series al alloys: Phase fraction diagrams[J].Journal of Mining&Metallurgy,2017,54:52-52.DOI:10.2298/JMMB170512052C.
[12] Kairy S K , Rometsch P A , Davies C H J ,et al.On the Intergranular Corrosion and Hardness Evolution of 6xxx Series Al Alloys as a Function of Si:Mg Ratio, Cu Content, and Aging Condition[J].Corrosion: The Journal of Science and Engineering, 2017(10):73.DOI:10.5006/2506.
[13] Wu X , Sun M , Hong L ,et al.Er-containing microalloyed aluminum alloys: a review[J].Journal of Materials Science, 2024, 59(22).DOI:10.1007/s10853-023-09185-w.
[14] Marola S , Fiore G , Battezzati L .Effect of Modifiers on the Microstructure of Rapidly Solidified AlSi10Mg Alloy[J].Metallurgical and Materials Transactions A, 2023, 54(2):624-633.DOI:10.1007/s11661-022-06907-8.
[15] Dai Y , Yan L , Hao J .Review on Micro-Alloying and Preparation Method of 7xxx Series Aluminum Alloys: Progresses and Prospects[J].Materials (Basel, Switzerland), 2022, 15(3).DOI:10.3390/ma15031216.
[16] Xu C , Xiao W , Zheng R ,et al. The synergic effects of Sc and Zr on the microstructure and mechanical pr-operties of Al-Si-Mg alloy[J].Materials & Design, 2015, 88(DEC.25):485-492.DOI:10.1016/j.matdes.2015.09.045.
[17] Santos A , Costa S , Pinto A M P .Effect of Sc Addi-tions on the Modification of Eutectic Si of As Cast Al-9wt%Si Alloy[J].Microscopy & Microanalysis, 2015, 21(S5):43-44.DOI:10.1017/S1431927615014026.
[18] Xu C , Wang F , Mudassar H ,et al.Effect of Sc and Sr on the Eutectic Si Morphology and Tensile Properties of Al-Si-Mg Alloy[J].Journal of Materials Engineering & Performance, 2017, 26(4):1605-1613.DOI:10.1007/s11665-017-2599-5.
[19] Yu-Chih,Tzeng,Chih-Ting,et al.Effects of trace Be and Sc addition on the thermal stability of Al-7Si-0.6Mg alloys[J].Materials Science & Engineering A Structural Materials Properties Misrostructure & Processing, 2014.
[20] Xu C , Xiao W , Hanada S ,et al.The effect of scandium addition on microstructure and mechanical properties of Al-Si-Mg alloy: A multi-refinement modifier[J].Materials Characterization, 2015, 110:160-169.DOI:10.1016/j.matchar.2015.10.030.
[21] Lu Z , Zhang L .Thermodynamic description of the quaternary Al-Si-Mg-Sc system and its application to the design of novel Sc-additional A356 a

lloys[J].Materials & Design,2017,116(feb.):427-437.DOI:10.1016/j.matdes.2016.12.034.

[22] Zhao Q, Huang H J, Yuan X G, et al. Aging precipitation and strengthening behavior of Al-Mg-Si alloy sheet containing Er and Zr element[J]. Trans. Mater. Heat Treat, 2015, 36(11): 40-46.

[23] Zheng D , Li J , Wei B ,et al.Sn-Sc microalloying-induced property improvement and micromechanisms of an Al-Mg-Si alloy[J].Journal of Materials Research and Technology,2023,27(000):18.DOI:10.1016/j.jmrt.2023.09.307.

[24] Deng, L., Zhang, H.-d., Li, G.-a., Tang, X.-f., Yi, P.-s., Liu, Z., Wang, X.-y., & Jin, J.-s. (2022). Processing map and hot deformation behavior of squeeze cast 6082 aluminum alloy. *Transactions of Nonferrous Metals Society of China, 32*(7), 2150–2163.

[25] Yi H J , Ding J , Ni C ,et al.Hot compression deformation behavior and processing maps of Al-0.5Mg-0.4Si-0.1Cu alloy[J].Journal of Materials Research and Technology, 2022.DOI:10.1016/j.jmrt.2022.07.027.

[26] Feng X , Wang Y , Huang Q ,et al.The dynamic recrystallization microstructure characteristics and the effects on static recrystallization and mechanical properties of Al-Mg-Si alloy[J].Materials Science & Engineering, A. Structural Materials: Properties, Misrostructure and Processing, 2024(May):899.

[27] Zhao Q , Li F , Zhu E ,et al.Understanding the isothermal compression behavior of Al-Mg-Si alloy based on hot deformation parameters and instability criteria[J].Materials Today Communications, 2024, 40:110074.DOI:10.1016/j.mtcomm.2024.110074.

[28] Liu S , Pan Q , Li H ,et al.Characterization of hot deformation behavior and constitutive modeling of Al-Mg-Si-Mn-Cr alloy[J].Journal of Materials Science, 2019(5):54.